

# Optimizing for an arbitrary Schrödinger cat state.

## I. Functionals and application to coherent dynamics

Matthias G. Krauss,<sup>1,2</sup> Christiane P. Koch,<sup>2</sup> and Daniel M. Reich<sup>2,\*</sup>

<sup>1</sup>*Theoretische Physik, Universität Kassel, Heinrich-Plett-Straße 40, 34132 Kassel, Germany*

<sup>2</sup>*Dahlem Center for Complex Quantum Systems and Fachbereich Physik, Freie Universität Berlin, Arnimallee 14, D-14195 Berlin, Germany*

A key task in the field of quantum optimal control is to encode physical targets into figures of merit to be used as optimization functionals. Here we derive a set of functionals for optimization towards an arbitrary cat state. We demonstrate the application of the functionals by optimizing the dynamics of a Kerr-nonlinear Hamiltonian with two-photon driving. Furthermore, we show the versatility of the framework by adapting the functionals towards optimization of maximally entangled cat states, applying it to a Jaynes-Cummings model. Finally, we identify the strategy of the obtained control fields and determine the quantum speed limit as a function of the cat state's excitation. Our results highlight the power of optimal control with functionals specifically crafted for complex physical tasks. They allow for optimizing the preparation of entangled cat states in more realistic settings, including, e.g., dissipative effects which we investigate in the companion paper.

### I. INTRODUCTION

Schrödinger cat states [1, 2] have been attracting a great deal of attention for the implementation of hardware-efficient qubit encodings [3, 4]. Recently, these include photonic [5] and superconducting quantum information [6, 7] architectures due to their intrinsic fault tolerance and suitability for quantum error correction. Various approaches have been proposed and implemented for their creation, involving, e.g., a set of fundamental logical gates [8, 9], homodyne detection [10, 11], adiabatic protocols [12, 13] or quantum reservoir engineering [14, 15]. Many of these approaches suffer from a long protocol time which in turn limits the speed in quantum information applications and makes the cat state generation susceptible to decoherence.

A powerful tool to obtain fast and robust state preparation protocols is quantum optimal control theory [16, 17]. It aims to determine suitable external controls for steering a physical system towards a particular goal, often by employing iterative numerical algorithms. The success of such algorithms crucially depends on choosing an appropriate optimization functional, i.e., a figure of merit encoding the optimization success by a single real number. An obvious choice for state-to-state optimizations is the overlap between the state generated by the optimized pulse and the target state. Such functionals have also been successfully employed for optimal control of cat state generation [18–20]. State overlap functionals only allow for optimization towards a single, specific state whereas in many applications it is often sufficient to obtain *any* cat state. The actual optimization target is then a set of states and not a single state. Since the goal of the optimization is encoded in the functional's extremal values [21], tailoring the optimization functional

to the underlying task helps to represent the physical target as faithfully as possible. This allows for maximal flexibility in finding optimal solutions which might be missed by too restrictive functionals. Such specifically crafted functionals for complex optimization tasks have proven to be very successful, e.g., in the optimization of individual optical cycles in laser cooling of molecules [22] or the optimization towards sets of entangling quantum gates [23, 24] instead of specific gates.

Here we derive an optimization functional which allows for optimization towards the entire set of cat states instead of only a specific element. By engineering a set of functional terms, which individually check for all desired properties of the target state, we are able to construct a composite functional which takes on its extremal, optimal value if and only if a cat state is obtained. We show that additional terms allow to tune the functional further for example towards targeting a specific displacement of the coherent states constituting the cat. Finally, we also demonstrate that the functional can be straightforwardly adapted for optimization of maximally entangled cats in a bipartite system. Such states are important in quantum sensing applications [25, 26] or to implement so-called flying qubits [27].

The paper is organized as follows. We begin in Sec. II by briefly introducing cat states as well as the basic framework of optimal control theory, using Krotov's algorithm as an example. At the end of Sec. II we present our construction of the functional for optimization towards arbitrary cat states and arbitrary maximally entangled cat states. Section III illustrates the application of the cat state functional for optimization in a Kerr-nonlinear oscillator with two-photon driving. In Sec. IV we present results for an example optimization towards maximally entangled cat states in a Jaynes-Cummings model and discuss which insight can be drawn from the optimization results regarding the role of the excitation of the cat state and the quantum speed limit. Finally, Sec. V concludes.

---

\* danreich@zedat.fu-berlin.de

## II. FRAMEWORK FOR TARGETING CAT STATES

Cat states are defined as a superposition of two coherent states  $|\alpha\rangle$  where the complex valued parameter  $\alpha$  describes the displacement in phase space, respectively the excitation, of the coherent states with respect to the ground state  $|0\rangle$  [1, 2]. In its most general form a cat state reads

$$|\psi_{\text{cat}}\rangle = \frac{1}{\mathcal{N}_\varphi} \left( |\alpha\rangle + e^{i\varphi} |-\alpha\rangle \right), \quad (1)$$

with  $\mathcal{N}_\varphi = \sqrt{2(1 + e^{-2|\alpha|^2} \cos(\varphi))}$  accounting for normalization. In the following, we refer to the relative phase  $\varphi$  between the two coherent states, as “superposition phase”. Note that it is also possible to consider superpositions of more than two coherent states, which are commonly referred to as multicomponent cat states [28]. However, in this paper we use the term “cat state” exclusively for two-component superpositions as the focus of our study.

Before we move to derive functionals optimizing towards an arbitrary cat state we briefly review Krotov’s method [29–31] which we employ for all numerical optimizations performed in this work.

### A. Optimization algorithm

Krotov’s method [29–31] is an iterative, monotonically convergent optimization algorithm using gradient information to achieve convergence. The optimization target typically consists of two parts,

$$J = J_T[\psi(T)] + \int_0^T J_t[\psi(t), \varepsilon(t)] dt, \quad (2)$$

where we assume a control problem described by a single Hilbert space state  $\psi(t)$  and a single control field  $\varepsilon(t)$ , commonly realized by external electromagnetic pulses. The first part of  $J_T$  depends only on the state at final time  $T$  and encodes the target to be reached at the end of the control pulse, whereas the intermediate time functional  $J_t$  describes further costs. In Krotov’s algorithm, the following cost functional is usually employed,

$$J_t[\psi(t), \varepsilon(t)] = \frac{\lambda_a}{S(t)} [\varepsilon(t) - \varepsilon_{\text{ref}}(t)]^2, \quad (3)$$

with the shape function  $S(t)$  ensuring that the optimized field is smoothly switched on and off. The reference field  $\varepsilon_{\text{ref}}(t)$  is commonly taken to be the field from the previous iteration. This choice allows the parameter  $\lambda_a$  to tune the step size of the optimization algorithm by penalizing large changes in the control field between iteration steps [32].

The update equation for the pulse in the iteration  $k+1$  of the algorithm is given by [31–33]

$$\varepsilon^{(k+1)}(t) = \varepsilon^{(k)}(t) + \frac{S(t)}{\lambda_a} \Im \left\{ \left\langle \chi^{(k)}(t) \left| \frac{\partial \hat{H}}{\partial \varepsilon} \right|_{\varepsilon^{(k+1)}(t)} \right| \psi^{(k+1)}(t) \right\rangle \right\}, \quad (4)$$

where  $\frac{\partial \hat{H}}{\partial \varepsilon}$  is the derivative of the Hamiltonian with respect to the control pulse  $\varepsilon$ . The  $|\chi^{(k)}(t)\rangle$  are often called costates. They are propagated backward in time according to the equation of motion,

$$\frac{d}{dt} |\chi^{(k)}(t)\rangle = \hat{H}[\varepsilon^{(k)}(t)] |\chi^{(k)}(t)\rangle, \quad (5)$$

with the boundary condition

$$|\chi^{(k)}(T)\rangle = -\nabla_{\langle \psi |} J_T \Big|_{t=T}. \quad (6)$$

The states  $|\psi^{(k+1)}(t)\rangle$  are obtained by solving the equation of motion

$$\frac{d}{dt} |\psi^{(k+1)}(t)\rangle = \hat{H}[\varepsilon^{(k+1)}(t)] |\psi^{(k+1)}(t)\rangle \quad (7a)$$

$$|\psi^{(k+1)}(0)\rangle = |\psi_0\rangle, \quad (7b)$$

where  $|\psi_0\rangle$  is the initial state of the system.

### B. Functional targeting a cat state

To construct a final time functional which allows for optimizing towards the set of cat states described by Eq. (1), we use the fact that the variance of an operator  $\hat{O}$  in a state  $|\psi\rangle$ ,

$$\Delta_\psi \hat{O} = \langle \psi | \hat{O}^\dagger \hat{O} | \psi \rangle - |\langle \psi | \hat{O} | \psi \rangle|^2, \quad (8)$$

is zero if and only if  $|\psi\rangle$  is an eigenstate of that operator. Coherent states are eigenstates of the annihilation operator,  $\hat{a} |\alpha\rangle = \alpha |\alpha\rangle$ . As a result, all cat states as defined in Eq. (1) are eigenstates of  $\hat{a}^2$ . Due to this property, we use the variance of  $\hat{a}^2$ ,

$$J_{\text{cs}}(\psi) = \Delta_\psi \hat{a}^2 = \left\langle \psi \left| (\hat{a}^\dagger)^2 \hat{a}^2 \right| \psi \right\rangle - \left| \langle \psi | \hat{a}^2 | \psi \rangle \right|^2, \quad (9)$$

as a starting point for the functional. However, cat states are not the only eigenstates of  $\hat{a}^2$ , such that a vanishing variance is a necessary but not sufficient condition to

identify an element from the set of cat states. Rather, all states of shape

$$|\psi_{a^2}\rangle = c_0 |\alpha\rangle + c_1 |-\alpha\rangle \quad (10)$$

with  $|c_0|^2 + |c_1|^2 + 2\Re\{c_0^*c_1\} \langle\alpha|-\alpha\rangle = 1$  and  $c_i \in \mathbb{C}$ , lead to  $J_{\text{cs}}(\psi) = 0$ . To obtain an expression whose minimal value is both necessary and sufficient to identify a cat state, we construct a composite functional with multiple terms,

$$J_{\text{T}}(\psi) = J_{\text{cs}}(\psi) + J_{\text{cat}}(\psi). \quad (11)$$

The first term is minimized if and only if the state is a superposition of  $|\alpha\rangle$  and  $|-\alpha\rangle$ , cf. Eq. (10) and the second term attains its minimum if and only if the desired subset of these superposition states is reached. We refer to  $J_{\text{cs}}(\psi)$  as ‘‘coherent state term’’ and to  $J_{\text{cat}}(\psi)$  as ‘‘cat term’’, due to their purpose in the overall functional. The specific form of the latter depends on which set of states should be targeted.

For example, optimizing towards the set of cat states defined in Eq. (1) can be achieved by choosing  $J_{\text{cat}}$  as

$$J_{\text{cat},\varphi}(\psi) = \left( \bar{a}^* \langle\psi|\hat{a}|\psi\rangle + \bar{a} \langle\psi|\hat{a}^\dagger|\psi\rangle \right)^2, \quad (12)$$

with  $\bar{a} \equiv \sqrt{\langle\psi|\hat{a}^2|\psi\rangle}$ . We prove in App. B, that  $J_{\text{cat},\varphi}(\psi)$  is indeed minimal if and only if  $|c_0|^2 = |c_1|^2$  in Eq. (10).

Another choice of  $J_{\text{cat}}$  which allows for  $\varphi$  being fixed to 0 or  $\pi$  is

$$J_{\text{cat},\pm}(\psi) = 1 - |\langle\psi|\hat{\Pi}_\pm|\psi\rangle|^2, \quad (13)$$

where

$$\hat{\Pi}_+ = \sum_{j \text{ even}} |j\rangle\langle j|, \quad \hat{\Pi}_- = \sum_{j \text{ odd}} |j\rangle\langle j|. \quad (14)$$

are the projectors onto the eigenspaces of the parity operator.  $\hat{\Pi}_+$  and  $\hat{\Pi}_-$  project onto even and odd cat states

$$|\psi_{\text{cat}}^\pm\rangle \propto |\alpha\rangle \pm |-\alpha\rangle, \quad (15)$$

with a superposition phase of 0(+) and  $\pi(-)$ , respectively, while not imposing any restriction on the value of  $\alpha$ .

A property shared by the functional terms in Eq. (9) and Eq. (12) is that their value is strongly suppressed for  $|\alpha| \rightarrow 0$ . This is due to the summands in both terms being proportional to  $|\alpha|^4$  and thus tending towards zero as  $|\alpha| \rightarrow 0$ . Therefore, the functional value is improved for smaller values of  $\alpha$ . Such a behavior can be problematic since many applications of cat states rely on a large displacement of the two coherent states in phase space, corresponding to larger  $|\alpha|$ . Examples for benefits of large displacements are increased sensing accuracy [34] or an improved robustness against errors in quantum information applications [35]. The tendency towards small

$|\alpha|$  can be amended by normalizing the coherent state term,

$$J_{\text{cs}}(\psi) = 1 - \frac{|\langle\psi|\hat{a}^2|\psi\rangle|^2}{\langle\psi|(\hat{a}^\dagger)^2\hat{a}^2|\psi\rangle}, \quad (16)$$

and the cat term for arbitrary superposition phases,

$$J_{\text{cat},\varphi}(\psi) = \frac{\langle\psi|\hat{a}|\psi\rangle}{\bar{a}} + \frac{\langle\psi|\hat{a}^\dagger|\psi\rangle}{\bar{a}^*}. \quad (17)$$

For the optimizations presented below, we always use the normalized expressions defined in Eqs. (16) and (17).

### C. Functional targeting an entangled cat state

The cat state functionals can be further adapted to more complex optimization targets. In this section we show how to extend our framework to target maximally entangled cat states in a bipartite system. Specifically, we consider a harmonic oscillator coupled to an atom described as a two-level system (TLS) – an ubiquitous physical setup in the field of cavity quantum electrodynamics and circuit quantum electrodynamics [2]. The corresponding optimization targets are given by states of the form

$$|\Psi_{\text{cat}}\rangle = \frac{1}{\sqrt{2}}(|b_+\rangle \otimes |\psi_{\text{cat}}^+\rangle + |b_-\rangle \otimes |\psi_{\text{cat}}^-\rangle), \quad (18)$$

where  $|\psi_{\text{cat}}^\pm\rangle$  is defined in Eq. (15) and  $|b_\pm\rangle$  denotes an arbitrary orthonormal basis of the TLS. In the spirit of allowing maximal flexibility, we again aim to derive a functional to optimize towards arbitrary maximally entangled cat states, i.e., the entire set of such states. In particular, we do not want to impose any restrictions on the basis states of the TLS involved in the superposition. However, if a specific basis on the TLS is desired, the functional can be easily adapted by introducing an additional term to the optimization functional. For example, the parity operators can be employed to project out one of the two summands constituting the entangled cat state in Eq. (18). Then, it is straightforward to fix the state  $|b_\pm\rangle$  by calculating the overlap with the desired basis state.

To generalize the final time functional, Eq. (11), to an entangled cat state in a bipartite system, we modify the operator used to calculate the variance,

$$\hat{a} \rightarrow \hat{A} \equiv \hat{\mathbb{1}} \otimes \hat{a}. \quad (19)$$

Thus, the coherent state term is replaced by

$$\tilde{J}_{\text{cs}}(\Psi) = \Delta_\Psi \hat{A}^2. \quad (20)$$

Similar to the discussion in Sec. II B, it is insufficient to use only the coherent state functional  $\tilde{J}_{\text{cs}}(\Psi)$  since it takes on its minimal values not only for the desired set

of states defined in Eq. (18), but for a larger set of states given by

$$|\Psi_{\text{ent}}\rangle = d_0(|g\rangle \otimes |\psi_{0,a^2}\rangle) + d_1(|e\rangle \otimes |\psi_{1,a^2}\rangle), \quad (21)$$

with  $|\psi_{j,a^2}\rangle$  being eigenstates of  $\hat{a}^2$  (cf. Eq. (10)) and  $d_i \in \mathbb{C}$  with  $|d_0|^2 + |d_1|^2 = 1$ . To amend this, we once again construct a composite functional, adding an additional term to restrict the set of states to exactly those of the form of  $|\Psi_{\text{cat}}\rangle$ . We accomplish this by exploiting the fact that the targeted states  $|\Psi_{\text{cat}}\rangle$  are maximally entangled. This means that the reduced states of the harmonic oscillator, respectively the TLS, take on the minimal purity value of  $\mathcal{P} = 0.5$ . For this reason we employ the following cat term tracking the subsystem purity,

$$J_{\text{cat}}(\Psi) = 2 \text{Tr}(\hat{\rho}_{\text{HO}}^2) - 1 = 2 \text{Tr}(\hat{\rho}_{\text{TLS}}^2) - 1, \quad (22)$$

where  $\hat{\rho}_{\text{HO}} = \text{Tr}_{\text{TLS}}[\hat{\rho}]$  and  $\hat{\rho}_{\text{TLS}} = \text{Tr}_{\text{HO}}[\hat{\rho}]$ .  $\text{Tr}_{\text{TLS}}[\cdot]$  and  $\text{Tr}_{\text{HO}}[\cdot]$  are the partial traces corresponding to the two-level system and the harmonic oscillator, respectively. Note that we have used the fact that  $\hat{\rho}$  is a pure state in the second equality. This assumption is valid since we only consider coherent dynamics in this study. In the companion paper [36] we take dissipation explicitly into account and show how to adjust the cat state term accordingly. Furthermore, as is commonly done in optimal control, we have renormalized  $J_{\text{cat}}(\Psi)$  such that it takes on values between zero and one. For the cat term in Eq. (22), we explicitly calculate the costates in App. A.

The cat term in Eq. (22) ensures both that the eigenstates of  $\hat{a}^2$ ,  $|\psi_{j,a^2}\rangle$  in the entangled cat state superposition are orthogonal to each other, i.e.,  $\langle\psi_{0,a^2}|\psi_{1,a^2}\rangle = 0$ , and that the prefactors in Eq. (21) are the same, i.e.,  $|d_0| = |d_1|$ . Thus, the combined functional,

$$J_T(\Psi) = \tilde{J}_{cs}(\Psi) + J_{\text{cat}}(\Psi), \quad (23)$$

takes on its minimal value only for states

$$|\Psi_{\text{ent}}\rangle = \frac{1}{\sqrt{2}}(|b_0\rangle \otimes |\psi_{0,a^2}\rangle + |b_1\rangle \otimes |\psi_{1,a^2}\rangle), \quad (24)$$

with  $\langle\psi_{0,a^2}|\psi_{1,a^2}\rangle = 0$  and  $|b_j\rangle$  being arbitrary orthogonal basis states of the TLS. Indeed, the states in Eq. (24) are equivalent to those in Eq. (18), which we prove in App. C.

### III. OPTIMIZATION RESULTS FOR A KERR-NONLINEAR RESONATOR

To demonstrate the application of the functional constructed in Sec. II B, we consider a Kerr-nonlinear resonator with two-photon driving. In the rotating frame, it reads

$$\hat{H}_{\text{Kerr}} = -K\hat{a}^\dagger\hat{a}^\dagger\hat{a}\hat{a} + \varepsilon(t)\hat{a}^2 + \varepsilon^*(t)(\hat{a}^\dagger)^2, \quad (25)$$

where  $K$  is the strength of the Kerr nonlinearity and  $\varepsilon(t)$  is the complex-valued amplitude of the two-photon drive.

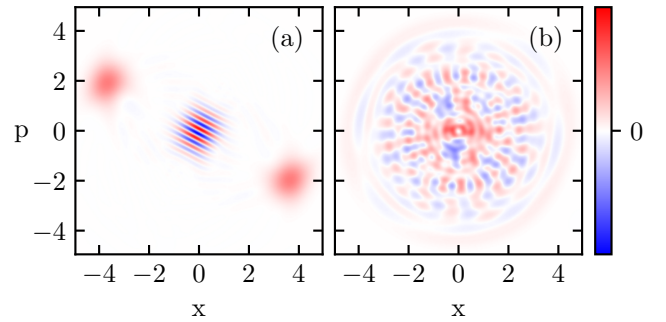


FIG. 1. Comparison of the optimization results for two different functionals. The plot shows the Wigner distribution of the final states obtained with the cat state functional described in Sec. II in (a) and with the state-to-state functional (Eq. (26)) in (b).

This Hamiltonian has recently been realized experimentally via coupled Josephson junctions [15]. In this setting, various protocols exist for the generation of cat states using this [37] or similar Hamiltonians [38, 39]. The set of reachable cat states in this system is limited by the two-photon drive in Eq. (25) and depends on the initial state since the driving only allows for direct transfer between next-nearest energy levels, i.e.,  $\Delta n = \pm 2$ . Therefore, when starting in the ground state  $|0\rangle$ , it is only possible to reach even-parity states. This means that only even cat states corresponding to a superposition phase  $\varphi = 0$  are reachable. If the initial state is not the ground state or – more generally – an element of the even-parity subspace, then even cat states are unreachable, as transitions between the two parity subspaces are forbidden under two-photon driving.

We compare the performance of a naive state-to-state optimization with our cat state optimization for the initial state  $|\psi_0\rangle = \frac{1}{\sqrt{2}}(|0\rangle + |1\rangle)$ . For the former optimization, we use the state-to-state functional,

$$J_{ss}(\psi(T)) = 1 - |\langle\psi(T)|\psi_{\text{tgt}}\rangle|. \quad (26)$$

with the target state being an even cat state  $|\psi_{\text{tgt}}\rangle = |\psi_{\text{cat}}^+\rangle$ , similar to Ref. [18]. We present results for  $\alpha = 1.5$ , but optimizations for different  $\alpha$  yield similar results. Since the initial state  $|\psi_0\rangle$  is not of even parity, it cannot evolve into an even cat state under two-photon driving. For the latter optimization, we use the cat state functional from Sec. II B with the cat term  $J_{\text{cat}}$  chosen as in Eq. (13) targeting an arbitrary element from the cat state set with an arbitrary superposition phase.

Figure 1 shows the Wigner distribution of the final states after optimization with both functionals. While the optimization result for the cat state functional (Fig. 1(a)) exhibits the classical phase space structure of a cat state, i.e., two coherent states with interference fringes in between them, the results of the state-to-state functional (Fig. 1(b)) do not resemble a cat state. To

quantify the distance between the optimized states and the set of cat states we define the “cat infidelity” to be the smallest infidelity between the final state and any element of the cat state set,

$$I_{\text{cat}}(\psi) = \min_{|\phi\rangle \in \{|\psi_{\text{cat}}\}} 1 - F(\phi, \psi), \quad (27)$$

where

$$F(\phi, \psi) = |\langle \phi | \psi \rangle| \quad (28)$$

is the state fidelity and  $\{|\psi_{\text{cat}}\}$  is the set of all cat states, which are described by Eq. (1). Using this definition, we obtain a cat infidelity of  $\approx 0.004$  for the optimization with the cat state functional and  $\approx 0.235$  for the naive state-to-state functional approach. This also confirms that the state obtained with the cat state functional is much closer to a cat state than the result achieved with the state-to-state functional. This further elucidates, that targeting even cat states via a state-to-state functional for this Hamiltonian can only succeed when starting from an even initial state, as discussed earlier.

Our results illustrate that the success of a naive state-to-state optimization hinges critically on the choice of the target state and can completely fail if, e.g., the symmetry of the system is not properly considered. Although it would be possible to amend such issues by sampling the parameter space of cat states and perform optimizations until success is achieved for some set of parameters, such an approach would be numerically very expensive. In contrast, using the functional introduced in Sec. II allows for a maximally general optimization target and thus makes scanning of the parameter space completely obsolete.

#### IV. OPTIMIZATION TOWARDS ENTANGLED CAT STATES IN A BIPARTITE SYSTEM

In this section we apply the functional from section Sec. II C to a system consisting of a harmonic oscillator coupled to a two-level system. One example for such a model is the dipolar transition between two circular Rydberg states interacting with a microwave cavity mode [2, 40]. For simplicity, we model this system by a resonant Jaynes-Cummings-Hamiltonian in the interaction picture. After applying the rotating wave approximation the Hamiltonian is given by

$$\hat{H}_{\text{JC}} = \hbar g(\hat{\sigma}_+ \otimes \hat{a} + \hat{\sigma}_- \otimes \hat{a}^\dagger) + \varepsilon^*(t)\hat{\sigma}_- \otimes \hat{\mathbb{1}} + \varepsilon(t)\hat{\sigma}_+ \otimes \hat{\mathbb{1}}, \quad (29)$$

where  $g$  describes the coupling strength between the harmonic oscillator and the two-level system and  $\varepsilon(t)$  is an external drive, which couples to the two-level system and can be realized by e.g. a microwave pulse. The eigenstates of  $\hat{H}_{\text{JC}}$  in Eq. (29) read

$$|n, \pm\rangle = \frac{1}{\sqrt{2}}(|0\rangle \otimes |n+1\rangle \pm |1\rangle \otimes |n\rangle), \quad (30)$$

with the corresponding eigenenergies  $E_n^\pm = \pm \hbar g \sqrt{n}$ . A more detailed introduction to the Jaynes-Cummings-Hamiltonian in the context of optimal control can be found, e.g., in Ref. [18].

To facilitate comparison between optimization results with different values of  $|\alpha|$ , we amend the functional by a third term  $J_{|\alpha|}(\Psi)$  which allows to target a particular value  $|\alpha|$ , called  $|\alpha_{\text{tgt}}|$  in the following. We accomplish this by defining a function of  $|\alpha|$ , which is minimal at the desired value  $|\alpha_{\text{tgt}}|$ . To compare the desired value  $|\alpha_{\text{tgt}}|$ , with the actual cat radius  $|\alpha|$  at final time  $T$  we use the expression

$$|\alpha|^4 = \langle \Psi(T) | (\hat{A}^\dagger)^2 \hat{A}^2 | \Psi(T) \rangle, \quad (31)$$

where  $\hat{A} = \hat{\mathbb{1}} \otimes \hat{a}$ , as above. Strictly speaking, this expression only yields a sensible value for  $|\alpha|$  if  $|\Psi(T)\rangle$  is an entangled cat states, which is only true if the optimization is fully converged through minimization of the other functional terms. Still, the value for  $|\alpha|$  obtained with Eq. (31) can be used as an estimate of the cat state radius, which in practice turns out to be a good approximation for states close to a cat state. Based on the estimate according to Eq. (31), we define the functional

$$J_{|\alpha|}(\Psi) = f(|\alpha|) = \frac{(|\alpha|^4 - |\alpha_{\text{tgt}}|^4)^2}{|\alpha_{\text{tgt}}|^8} + \frac{(|\alpha| - |\alpha_{\text{tgt}}|)^2}{|\alpha_{\text{tgt}}|^2}. \quad (32)$$

Note that any function  $f$  with a unique minimum at the desired value of  $|\alpha_{\text{tgt}}|$  could be chosen but the choice in Eq. (32) proves to be particularly suitable since it possesses high gradients for both small and large arguments. This helps accelerating convergence during the optimization both far away and close to the target value.

Using the functional  $J_{\text{T}}(\psi) = J_{\text{cs}}(\psi) + J_{\text{cat}}(\psi) + J_{|\alpha|}(\psi)$  we have performed numerical optimizations towards cat states with  $|\alpha_{\text{tgt}}| = 1$  and  $|\alpha_{\text{tgt}}| = 2$ , respectively, starting from the ground state of the atom-cavity system. For both values of  $|\alpha|$  we have obtained states with cat infidelities of  $I_{\text{cat}}(|\Psi(T)\rangle) < 10^{-3}$ , where we use the same definition as in Eq. (27), although this infidelity is now calculated with respect to the set of maximally entangled cat states defined in Eq. (18) to match the optimization goal. In Fig. 2, we show the spectra of the optimized pulses. Both spectra exhibit sharp peaks located at the transition frequencies between the eigenstates of the atom-cavity system  $|n, \pm\rangle$  (cf. Eq. (30)) of the drift Hamiltonian  $\hat{H}_{\text{JC}}$  with adjacent  $n$ , indicated by dashed lines in Fig. 2. Since the two-level system is driven, these are the only direct transitions between atom and cavity. In turn this allows for increasing or decreasing the number of excitations in the cavity by  $\Delta n = \pm 1$  due to the interaction. It also explains why we observe spectral broadening when optimizing for cat states with larger  $\alpha$ . Such cat states require higher levels of the harmonic oscillator to be populated and thus higher-level transitions between the eigenstates of the atom-cavity system need to be driven by the pulse. The transition frequencies between  $n$  and  $n+1$  become either  $\Delta\omega \propto \sqrt{n+1} + \sqrt{n}$

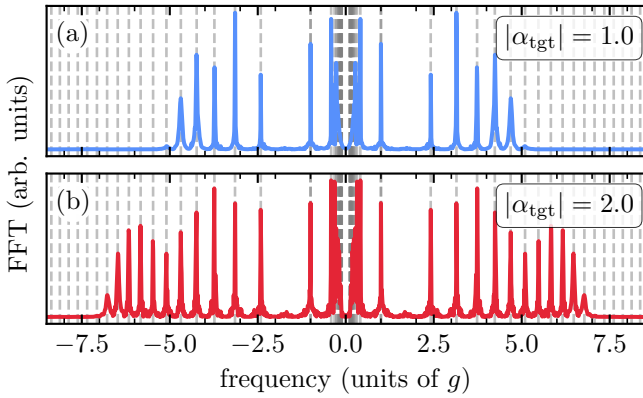


FIG. 2. Spectra of the optimized pulses for optimization towards maximally entangled cat states with  $|\alpha_{\text{tgt}}| = 1$  (top) and  $|\alpha_{\text{tgt}}| = 2$  (bottom). The dashed lines indicate the transition frequencies between the eigenstates  $|n, \pm\rangle$  of the drift Hamiltonian, defined in Eq. (30).

for  $|n, \pm\rangle \rightarrow |n+1, \pm\rangle$ , which we call type-(i) transitions or  $\Delta\omega \propto \sqrt{n+1} - \sqrt{n}$  for  $|n, \pm\rangle \rightarrow |n+1, \mp\rangle$ , which we call type-(ii) transitions. Since the latter frequencies tend towards zero with larger  $n$ , the type-(ii) transition frequencies become more and more difficult to resolve for a finite pulse duration. This only leaves the optimization algorithm to target the larger type-(i) transition frequencies to address higher-level transitions. Comparing the spectrum obtained for  $|\alpha_{\text{tgt}}| = 1.0$  in Fig. 2(a) and the spectrum for  $|\alpha_{\text{tgt}}| = 2.0$  in Fig. 2(b) confirms this interpretation. Indeed, the pulse in Fig. 2(b) contains larger frequency components in comparison to the pulse in Fig. 2(a) and exhibits a broader spectrum.

We now inspect the optimized pulse obtained for  $|\alpha_{\text{tgt}}| = 2.0$  in greater detail, noting that the optimization strategy obtained for  $|\alpha_{\text{tgt}}| = 1.0$  turns out to be very similar. Figure 3(c) depicts the real part of the optimized pulse in time domain, showing a consistent increase of the instantaneous pulse frequency with time. This behavior can be further elucidated with a Gabor transform of the pulse,

$$G_{\sigma}(\tau, \omega) \propto \int_{-\infty}^{\infty} e^{-\frac{(\tau-t)^2}{2\sigma^2}} e^{i\omega t} \varepsilon(t) dt, \quad (33)$$

shown in Fig. 3(b) with  $\sigma = \frac{T}{4\sqrt{2\pi}}$ . The Gabor transform reveals how the frequency components of the pulse change with time. For visual aid, the spectrum of the pulse from Fig. 2(b) is plotted again in Fig. 3(a). Indeed, the time-frequency distribution in Fig. 3(b) exhibits mainly contributions at the transition frequencies of the Jaynes-Cummings model. Additionally, the optimized pulse contains only a few frequency components at the beginning, with more - and in particular larger - frequencies added over time. This gradual driving of higher frequency components generates a population ascent towards higher levels, ultimately yielding the desired distribution.

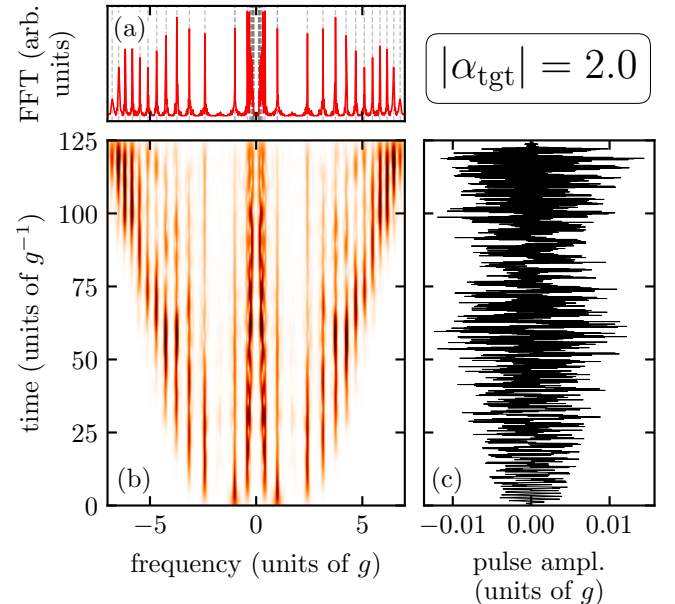


FIG. 3. Detailed analysis of the optimized pulse towards  $|\alpha_{\text{tgt}}| = 2.0$  showing the pulse in time domain (c), in frequency domain (a) and a time-frequency distribution (b) calculated via the Gabor transform. All quantities are expressed in units of the coupling strength  $g$ .

The pulse duration is an important property of an optimal control solution. It determines whether an operation can be carried out and influences the impact of dissipation. Specifically, finding the minimal time required to implement the physical target can help to limit the role of dissipative effects. Alternatively, dissipation can be included in the model - an approach that is followed in our companion paper [36]. Here, we restrict ourselves to coherent dynamics and use the functional developed in Sec. II C to investigate how fast cat states can be prepared for a Jaynes-Cummings Hamiltonian. The determination of the shortest time for generating or transforming states is an important task of optimal control theory. The resulting quantity is called the quantum speed limit [41–45], which is usually determined by a set of optimizations with varying pulse durations. The shortest pulse duration at which the objective can still be reliably reached is then used as an estimate for the quantum speed limit [43, 45].

Since the cat state functional is fairly complex, reaching convergence proved difficult in some of our calculations. Particularly the presence of plateaus in the optimization landscape posed an appreciable problem during some optimizations. These plateaus lead to asymptotically slow convergence if the value of  $\lambda_a$ , cf. Eq. (4), is kept constant during the optimization. Hence, we have employed an additional line search inside Krotov's method to find the best value for the step size parameter  $\lambda_a$  in each optimization step. With this modification, we have reliably obtained good convergence despite the

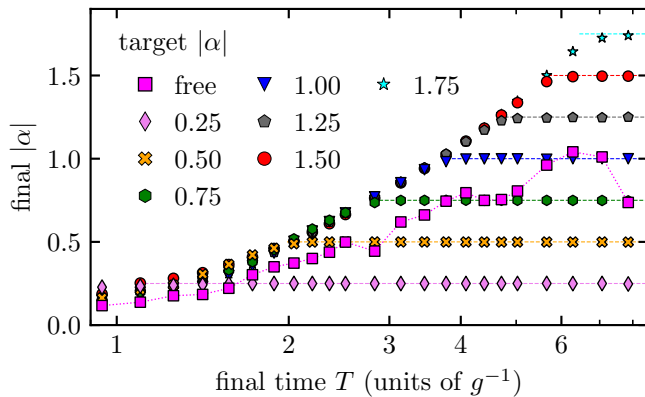


FIG. 4. The final value of  $|\alpha|$  plotted against the pulse duration  $T$  for different optimizations. The different marker styles indicate optimizations performed with different target values  $|\alpha_{\text{tgt}}|$ . The dashed auxiliary lines on the right, colored with the same color as the marker styles, are added to guide the eye.

functional’s complexity. The results for the optimizations with different pulse durations are depicted in Fig. 4. All data exhibit a similar trend, as the final value  $|\alpha|$ , cf. Eq. (31), steadily increases for small values of  $T$  and saturates at the desired value as soon as the pulse duration crosses a certain threshold. Once this threshold is reached, the optimization attains the desired value reliably. The smallest duration  $T_{\text{QSL}}^\alpha$  at which  $|\alpha|$  reaches  $|\alpha_{\text{tgt}}|$  increases with the desired target value  $|\alpha_{\text{tgt}}|$ . This suggests that  $T_{\text{QSL}}^\alpha$  indeed represents the quantum speed limit. The increase of  $T_{\text{QSL}}^\alpha$  with  $|\alpha_{\text{tgt}}|$  can be directly justified with our previous findings in Fig. 3, showing that higher levels need to be sequentially populated and thus longer times are needed for higher excitation of the cat state.

We have also performed optimizations towards entangled cat states without prescribing a target value for  $|\alpha|$ , i.e., without the term  $J_{|\alpha|}$ . The obtained “free” optimization results are plotted as magenta squares in Fig. 4. As expected, the final values of the cat state radii  $|\alpha|$  stay below all curves indicating the quantum speed limit for a given value of  $|\alpha|$ . However, the final values  $|\alpha|$  do not always increase with larger pulse durations for the “free” optimization, whereas the quantum speed limit continuously increases towards larger values of  $|\alpha_{\text{tgt}}|$ . This is in accordance with our previous findings in Fig. 3, showing that higher levels need to be populated one after another. Since larger excitations of the cat state, i.e., larger  $|\alpha|$ , require more transitions to higher levels, the larger time required to reach the target is not surprising.

## V. CONCLUSIONS

We have developed an optimization framework to target cat states and entangled cat states in bipartite sys-

tems. The corresponding functionals target the whole set of cat states instead of individual elements from this set. As a result, they provide the maximal flexibility for the optimization algorithm to steer the system towards the most suitable state from the set in a given physical setup. The composite functionals consist of several terms, which separately check whether the state is an eigenstate of the annihilation operator, whether it is an equally weighted superposition, and, in case of a bipartite entangled cat, whether the two subsystems are maximally entangled. Moreover, we have shown how to adjust the functionals to specify particular cat state properties, such as a desired displacement of the coherent states constituting the cat superposition.

We have performed example optimizations using these functionals for a Kerr-nonlinear oscillator with two-photon driving. By directly comparing their performance with a naive state-to-state approach, we have been able to show that our framework reliably finds cat states, whereas the state-to-state approach needs to be manually adjusted to a reachable state in advance. This demonstrates the power of the cat state functionals which allow to avoid analyzing the reachable set of cat states in advance. Furthermore, we have successfully applied the functionals for maximally entangled bipartite cat states in an archetypical Jaynes-Cummings model. We have analyzed the structure of the optimized pulses which show a consecutive transfer of population towards higher energy levels as control mechanism. Moreover, we have investigated how fast cat states can be prepared and determined the quantum speed limit which we found to be directly connected to the excitation of the cat states, i.e., to the cat radius.

In the future the functionals could be further adapted to target more complex sets of states, for example, multicomponent cat states [28] or (entangled) multipartite cat states [25, 27, 46]. Another potential future avenue of our work is to extend the framework to the generation of squeezed states or squeezed cat states, which have recently attracted interest in quantum error correcting codes [47].

## ACKNOWLEDGMENTS

Financial support from the federal state of Hesse, Germany via the SMolBits project within the LOEWE program is gratefully acknowledged.

## Appendix A: Calculation of the costate

In the following, we briefly summarize the calculation of the costates,

$$|\chi\rangle = -\nabla_{\langle\psi|} J_T = -\frac{\partial J}{\partial \langle\Psi|} \Big|_{t=T}. \quad (\text{A1})$$

For the terms presented in Sec. II, most of the costates can be directly calculated by using the relation

$$\frac{\partial}{\partial \langle\Psi|} \text{Tr}(\hat{O}\hat{\rho}) = \frac{\partial}{\partial \langle\Psi|} \langle\psi|\hat{O}|\psi\rangle = \hat{O}|\psi\rangle, \quad (\text{A2})$$

where  $\hat{\rho} = |\psi\rangle\langle\psi|$ . However, the calculation of the costates for the cat term in Eq. (22) is not as straightforward. To calculate the derivative, we first express Eq. (22) as

$$J_P(\Psi) \equiv J_P(\Psi_1, \Psi_2) \Big|_{\Psi_1=\Psi_2=\Psi} \quad (\text{A3})$$

$$= 2 \text{Tr}(\hat{\rho}_{1,\text{HO}} \hat{\rho}_{2,\text{HO}}) \Big|_{\hat{\rho}_1=\hat{\rho}_2=\hat{\rho}} - 1 \quad (\text{A4})$$

with  $\hat{\rho}_{i,\text{HO}} = \text{Tr}_{\text{TLS}}[\hat{\rho}_i]$ . Using this relation, we calculate the costate of the cat term  $|\chi_P\rangle$  as

$$\begin{aligned} |\chi_P\rangle &= -\frac{\partial J_P}{\partial \langle\Psi|} \Big|_{t=T} = -\left( \frac{\partial J_P}{\partial \langle\Psi_1|} + \frac{\partial J_P}{\partial \langle\Psi_2|} \right) \Big|_{\Psi_1=\Psi_2=\Psi} \\ &= -\left( \left( 2 \frac{\partial}{\partial \langle\Psi_1|} \text{Tr}((\hat{\rho}_{2,\text{HO}} \otimes \hat{\mathbb{1}}_{\text{TLS}}) \hat{\rho}_1) \right) \right. \\ &\quad \left. + \left( 2 \frac{\partial}{\partial \langle\Psi_2|} \text{Tr}((\hat{\rho}_{1,\text{HO}} \otimes \hat{\mathbb{1}}_{\text{TLS}}) \hat{\rho}_2) \right) \right) \Big|_{\Psi_1=\Psi_2=\Psi} \\ &= -\left( 2(\hat{\rho}_{2,\text{HO}} \otimes \hat{\mathbb{1}}_{\text{TLS}}) |\Psi_1(T)\rangle \right. \\ &\quad \left. + 2(\hat{\rho}_{1,\text{HO}} \otimes \hat{\mathbb{1}}_{\text{TLS}}) |\Psi_2(T)\rangle \right) \Big|_{\Psi_1=\Psi_2=\Psi} \\ &= -4(\hat{\rho}_{\text{HO}} \otimes \hat{\mathbb{1}}_{\text{TLS}}) |\Psi(T)\rangle. \quad (\text{A5}) \end{aligned}$$

## Appendix B: Derivation of the cat term for arbitrary superposition phases

We show that an eigenstate of  $\hat{a}^2$  (cf. Eq. (10)) is of the form of Eq. (1) if and only if

$$\|\bar{a}|\psi_{a^2}\rangle - \hat{a}|\psi_{a^2}\rangle\|^2 = \|\bar{a}|\psi_{a^2}\rangle + \hat{a}|\psi_{a^2}\rangle\|^2, \quad (\text{B1})$$

where  $\bar{a} \equiv \sqrt{\langle\psi_{a^2}|\hat{a}^2|\psi_{a^2}\rangle}$ , which becomes  $\bar{a} = \sqrt{\alpha^2} = \alpha$  if the state is an eigenstate of  $\hat{a}^2$ . Expanding both sides of the equation yields

$$\begin{aligned} \bar{a}|\psi_{a^2}\rangle - \hat{a}|\psi_{a^2}\rangle &= \\ &= c_1\alpha|\alpha\rangle + c_2\alpha|-\alpha\rangle - c_1\alpha|\alpha\rangle + c_2\alpha|-\alpha\rangle \\ &= 2c_2\alpha|-\alpha\rangle, \\ \bar{a}|\psi_{a^2}\rangle + \hat{a}|\psi_{a^2}\rangle &= \\ &= c_1\alpha|\alpha\rangle + c_2\alpha|-\alpha\rangle + c_1\alpha|\alpha\rangle - c_2\alpha|-\alpha\rangle \\ &= 2c_1\alpha|\alpha\rangle. \end{aligned}$$

This implies

$$\begin{aligned} \|\bar{a}|\psi_{a^2}\rangle - \hat{a}|\psi_{a^2}\rangle\|^2 &= 4|c_2|^2|\alpha|^2, \\ \|\bar{a}|\psi_{a^2}\rangle + \hat{a}|\psi_{a^2}\rangle\|^2 &= 4|c_1|^2|\alpha|^2, \end{aligned}$$

such that Eq. (B1) reduces to

$$4|c_2|^2|\alpha|^2 = 4|c_1|^2|\alpha|^2 \iff |c_2|^2 = |c_1|^2$$

as desired. By calculating the state norms, Eq. (B1) can be further simplified to

$$\begin{aligned} \|\bar{a}|\psi_{a^2}\rangle \pm \hat{a}|\psi_{a^2}\rangle\|^2 &= \\ &= |\bar{a}|^2 \pm \bar{a}^* \langle\psi_{a^2}|\hat{a}|\psi_{a^2}\rangle \\ &\quad \pm \bar{a} \langle\psi_{a^2}|\hat{a}^\dagger|\psi_{a^2}\rangle + \langle\psi_{a^2}|\hat{a}^\dagger\hat{a}|\psi_{a^2}\rangle \quad (\text{B2}) \end{aligned}$$

which yields the condition

$$\bar{a}^* \langle\psi_{a^2}|\hat{a}|\psi_{a^2}\rangle + \bar{a} \langle\psi_{a^2}|\hat{a}^\dagger|\psi_{a^2}\rangle \stackrel{!}{=} 0, \quad (\text{B3})$$

that is used for the cat term in Eq. (12).

## Appendix C: Proof for the equivalence of Eq. (18) and Eq. (23)

In Sec. II C a functional is constructed which allows for optimizing towards states of the form given in Eq. (23). At first glance, this appears to be a different form compared to the desired entangled cat states in Eq. (18). In the following we show that both expressions are indeed equivalent. To this end, we first write the eigenstate of the annihilation operator  $\hat{a}^2$  defined in Eq. (10) as

$$|\psi_{a^2}\rangle = c_0|\alpha\rangle + c_1|-\alpha\rangle = d_+|\psi_{\text{cat}}^+\rangle + d_-|\psi_{\text{cat}}^-\rangle, \quad (\text{C1})$$

where  $|d_+|^2 + |d_-|^2 = 1$ ,  $d_\pm \in \mathbb{C}$ . Using this, we rewrite Eq. (24) as

$$\begin{aligned} |\Psi_{\text{ent}}\rangle &= \frac{1}{\sqrt{2}}(|b_0\rangle \otimes |\psi_{0,a^2}\rangle + |b_1\rangle \otimes |\psi_{1,a^2}\rangle) \\ &= \frac{1}{\sqrt{2}}(|b_0\rangle \otimes (d_{0+}|\psi_{\text{cat}}^+\rangle + d_{0-}|\psi_{\text{cat}}^-\rangle) \\ &\quad + |b_1\rangle \otimes (d_{1+}|\psi_{\text{cat}}^+\rangle + d_{1-}|\psi_{\text{cat}}^-\rangle)) \\ &= \frac{1}{\sqrt{2}}(e^{i\Theta_0}|b_0\rangle \otimes (\cos\varphi|\psi_{\text{cat}}^+\rangle + \sin\varphi e^{i\theta}|\psi_{\text{cat}}^-\rangle) \\ &\quad + e^{i\Theta_1}|b_1\rangle \otimes (\sin\varphi|\psi_{\text{cat}}^+\rangle - \cos\varphi e^{i\theta}|\psi_{\text{cat}}^-\rangle)). \quad (\text{C2}) \end{aligned}$$

Since  $\langle\psi_{0,a^2}|\psi_{1,a^2}\rangle = 0$ , we can reexpress the prefactors of the cat states as

$$\begin{aligned} d_{0+} &= e^{i\Theta_0} \cos\varphi, & d_{0-} &= e^{i\Theta_0} e^{i\theta} \sin\varphi, \\ d_{1+} &= e^{i\Theta_1} \sin\varphi, & d_{1-} &= -e^{i\Theta_1} e^{i\theta} \cos\varphi, \end{aligned}$$

with  $\varphi, \theta, \Theta_i \in \mathbb{R}$ . Using these relations, we rewrite (C2) as

$$\begin{aligned}
|\Psi_{\text{ent}}\rangle &= \frac{1}{\sqrt{2}} \left( e^{i\Theta_0} |b_0\rangle \otimes (\cos \varphi |\psi_{\text{cat}}^+\rangle + \sin \varphi e^{i\theta} |\psi_{\text{cat}}^-\rangle) \right. \\
&\quad \left. + e^{i\Theta_1} |b_1\rangle \otimes (\sin \varphi |\psi_{\text{cat}}^+\rangle - \cos \varphi e^{i\theta} |\psi_{\text{cat}}^-\rangle) \right) \\
&= \frac{1}{\sqrt{2}} \left( (e^{i\Theta_0} \cos \varphi |b_0\rangle + e^{i\Theta_1} \sin \varphi |b_1\rangle) \otimes |\psi_{\text{cat}}^+\rangle \right. \\
&\quad \left. + e^{i\theta} (e^{i\Theta_0} \sin \varphi |b_0\rangle - e^{i\Theta_1} \cos \varphi |b_1\rangle) \otimes |\psi_{\text{cat}}^-\rangle \right) \\
&\equiv \frac{1}{\sqrt{2}} \left( |b_+\rangle \otimes |\psi_{\text{cat}}^+\rangle + |b_-\rangle \otimes |\psi_{\text{cat}}^-\rangle \right). \quad (\text{C3})
\end{aligned}$$

Thus, the state obtained by optimizing the functional in Eq. (23) is an entangled cat state as defined in Eq. (18).

- 
- [1] R. J. Glauber, Coherent and Incoherent States of the Radiation Field, *Phys. Rev.* **131**, 2766 (1963).
- [2] S. Haroche and J.-M. Raimond, *Exploring the Quantum: Atoms, Cavities and Photons*, Oxford Graduate Texts (Oxford University Press, Oxford ; New York, 2006).
- [3] S. Glancy and H. M. de Vasconcelos, Methods for producing optical coherent state superpositions, *J. Opt. Soc. Am. B* **25**, 712 (2008).
- [4] M. Mirrahimi, Cat-qubits for quantum computation, *Comptes Rendus Physique* **17**, 778 (2016).
- [5] Y.-H. Chen, R. Stassi, W. Qin, A. Miranowicz, and F. Nori, Fault-Tolerant Multiqubit Geometric Entangling Gates Using Photonic Cat-State Qubits, *Phys. Rev. Applied* **18**, 024076 (2022).
- [6] A. Grimm, N. E. Frattini, S. Puri, S. O. Mundhada, S. Touzard, M. Mirrahimi, S. M. Girvin, S. Shankar, and M. H. Devoret, Stabilization and operation of a Kerr-cat qubit, *Nature* **584**, 205 (2020).
- [7] Q.-P. Su, Y. Zhang, and C.-P. Yang, Single-step implementation of a hybrid controlled-not gate with one superconducting qubit simultaneously controlling multiple target cat-state qubits, *Phys. Rev. A* **105**, 062436 (2022).
- [8] B. Vlastakis, G. Kirchmair, Z. Leghtas, S. E. Nigg, L. Frunzio, S. M. Girvin, M. Mirrahimi, M. H. Devoret, and R. J. Schoelkopf, Deterministically Encoding Quantum Information Using 100-Photon Schrödinger Cat States, *Science* **342**, 607 (2013).
- [9] C. Wang, Y. Y. Gao, P. Reinhold, R. W. Heeres, N. Ofek, K. Chou, C. Axline, M. Reagor, J. Blumoff, K. M. Sliwa, L. Frunzio, S. M. Girvin, L. Jiang, M. Mirrahimi, M. H. Devoret, and R. J. Schoelkopf, A Schrödinger cat living in two boxes, *Science* **352**, 1087 (2016).
- [10] A. Ourjoumtsev, R. Tualle-Broui, J. Laurat, and P. Grangier, Generating Optical Schrödinger Kittens for Quantum Information Processing, *Science* **312**, 83 (2006).
- [11] A. Ourjoumtsev, H. Jeong, R. Tualle-Broui, and P. Grangier, Generation of optical ‘Schrödinger cats’ from photon number states, *Nature* **448**, 784 (2007).
- [12] T. Hatomura, Shortcuts to adiabatic cat-state generation in bosonic Josephson junctions, *New J. Phys.* **20**, 015010 (2018).
- [13] Y.-H. Chen, W. Qin, X. Wang, A. Miranowicz, and F. Nori, Shortcuts to Adiabaticity for the Quantum Rabi Model: Efficient Generation of Giant Entangled Cat States via Parametric Amplification, *Phys. Rev. Lett.* **126**, 023602 (2021).
- [14] C. Arenz, C. Cormick, D. Vitali, and G. Morigi, Generation of two-mode entangled states by quantum reservoir engineering, *J. Phys. B: At. Mol. Opt. Phys.* **46**, 224001 (2013).
- [15] Z. Leghtas, S. Touzard, I. M. Pop, A. Kou, B. Vlastakis, A. Petrenko, K. M. Sliwa, A. Narla, S. Shankar, M. J. Hatridge, M. Reagor, L. Frunzio, R. J. Schoelkopf, M. Mirrahimi, and M. H. Devoret, Confining the state of light to a quantum manifold by engineered two-photon loss, *Science* **347**, 853 (2015).
- [16] S. J. Glaser, U. Boscain, T. Calarco, C. P. Koch, W. Köckenberger, R. Kosloff, I. Kuprov, B. Luy, S. Schirmer, T. Schulte-Herbrüggen, D. Sugny, and F. K. Wilhelm, Training Schrödinger’s cat: Quantum optimal control: Strategic report on current status, visions and goals for research in Europe, *Eur. Phys. J. D* **69**, 279 (2015).
- [17] C. P. Koch, U. Boscain, T. Calarco, G. Dirr, S. Filipp, S. J. Glaser, R. Kosloff, S. Montangero, T. Schulte-Herbrüggen, D. Sugny, and F. K. Wilhelm, Quantum optimal control in quantum technologies. Strategic report on current status, visions and goals for research in Europe, *EPJ Quantum Technol.* **9**, 19 (2022).
- [18] K. Rojan, D. M. Reich, I. Dotsenko, J.-M. Raimond, C. P. Koch, and G. Morigi, Arbitrary-quantum-state preparation of a harmonic oscillator via optimal control, *Phys. Rev. A* **90**, 023824 (2014).
- [19] N. Ofek, A. Petrenko, R. Heeres, P. Reinhold, Z. Leghtas, B. Vlastakis, Y. Liu, L. Frunzio, S. M. Girvin, L. Jiang, M. Mirrahimi, M. H. Devoret, and R. J. Schoelkopf, Extending the lifetime of a quantum bit with error correction in superconducting circuits, *Nature* **536**, 441 (2016).
- [20] J.-J. Xue, K.-H. Yu, W.-X. Liu, X. Wang, and H.-R. Li, Fast generation of cat states in Kerr nonlinear resonators via optimal adiabatic control, *New J. Phys.* **24**, 053015 (2022).
- [21] C. P. Koch, Controlling open quantum systems: Tools, achievements, and limitations, *J. Phys.: Condens. Matter*

- 28**, 213001 (2016).
- [22] D. M. Reich and C. P. Koch, Cooling molecular vibrations with shaped laser pulses: Optimal control theory exploiting the timescale separation between coherent excitation and spontaneous emission, *New J. Phys.* **15**, 125028 (2013).
- [23] M. M. Müller, D. M. Reich, M. Murphy, H. Yuan, J. Vala, K. B. Whaley, T. Calarco, and C. P. Koch, Optimizing entangling quantum gates for physical systems, *Phys. Rev. A* **84**, 042315 (2011).
- [24] P. Watts, J. Vala, M. M. Müller, T. Calarco, K. B. Whaley, D. M. Reich, M. H. Goerz, and C. P. Koch, Optimizing for an arbitrary perfect entangler. I. Functionals, *Phys. Rev. A* **91**, 062306 (2015).
- [25] W. J. Munro, K. Nemoto, G. J. Milburn, and S. L. Braunstein, Weak-force detection with superposed coherent states, *Phys. Rev. A* **66**, 023819 (2002).
- [26] M. Penasa, S. Gerlich, T. Rybarczyk, V. Métillon, M. Brune, J. M. Raimond, S. Haroche, L. Davidovich, and I. Dotsenko, Measurement of a microwave field amplitude beyond the standard quantum limit, *Phys. Rev. A* **94**, 022313 (2016).
- [27] Z. Wang, Z. Bao, Y. Wu, Y. Li, W. Cai, W. Wang, Y. Ma, T. Cai, X. Han, J. Wang, Y. Song, L. Sun, H. Zhang, and L. Duan, A flying Schrödinger's cat in multipartite entangled states, *Sci. Adv.* **8**, eabn1778 (2022).
- [28] M. Bergmann and P. van Loock, Quantum error correction against photon loss using multicomponent cat states, *Phys. Rev. A* **94**, 042332 (2016).
- [29] V. Krotov, *Global Methods in Optimal Control Theory* (CRC Press, 1995).
- [30] A. I. Konnov and V. F. Krotov, On global methods of successive improvement of controll processes, *Autom. Remote Control* **60**, 1427 (1999).
- [31] M. Goerz, D. Basilewitsch, F. Gago-Encinas, M. G. Krauss, K. P. Horn, D. M. Reich, and C. Koch, Krotov: A Python implementation of Krotov's method for quantum optimal control, *SciPost Phys.* **7**, 080 (2019).
- [32] J. P. Palao and R. Kosloff, Optimal control theory for unitary transformations, *Phys. Rev. A* **68**, 062308 (2003).
- [33] D. M. Reich, M. Ndong, and C. P. Koch, Monotonically convergent optimization in quantum control using Krotov's method, *J. Chem. Phys.* **136**, 104103 (2012).
- [34] P. T. Cochrane, G. J. Milburn, and W. J. Munro, Macroscopically distinct quantum-superposition states as a bosonic code for amplitude damping, *Phys. Rev. A* **59**, 2631 (1999).
- [35] M. Mirrahimi, Z. Leghtas, V. V. Albert, S. Touzard, R. J. Schoelkopf, L. Jiang, and M. H. Devoret, Dynamically protected cat-qubits: A new paradigm for universal quantum computation, *New J. Phys.* **16**, 045014 (2014).
- [36] M. G. Krauss, D. M. Reich, and C. P. Koch, Optimizing for an arbitrary schrödinger cat state. II. Application in the presence of dissipation, TBD (2022).
- [37] S. Puri, S. Boutin, and A. Blais, Engineering the quantum states of light in a Kerr-nonlinear resonator by two-photon driving, *npj Quantum Inf* **3**, 18 (2017).
- [38] N. Bartolo, F. Minganti, W. Casteels, and C. Ciuti, Exact steady state of a Kerr resonator with one- and two-photon driving and dissipation: Controllable Wigner-function multimodality and dissipative phase transitions, *Phys. Rev. A* **94**, 033841 (2016).
- [39] F. Minganti, N. Bartolo, J. Lolli, W. Casteels, and C. Ciuti, Exact results for Schrödinger cats in driven-dissipative systems and their feedback control, *Sci Rep* **6**, 26987 (2016).
- [40] J. M. Raimond, M. Brune, and S. Haroche, Manipulating quantum entanglement with atoms and photons in a cavity, *Rev. Mod. Phys.* **73**, 565 (2001).
- [41] K. Bhattacharyya, Quantum decay and the Mandelstam-Tamm-energy inequality, *J. Phys. A: Math. Gen.* **16**, 2993 (1983).
- [42] N. Margolus and L. B. Levitin, The maximum speed of dynamical evolution, *Physica D: Nonlinear Phenomena* **120**, 188 (1998).
- [43] T. Caneva, M. Murphy, T. Calarco, R. Fazio, S. Montangero, V. Giovannetti, and G. E. Santoro, Optimal Control at the Quantum Speed Limit, *Phys. Rev. Lett.* **103**, 240501 (2009).
- [44] L. B. Levitin and T. Toffoli, Fundamental Limit on the Rate of Quantum Dynamics: The Unified Bound Is Tight, *Phys. Rev. Lett.* **103**, 160502 (2009).
- [45] M. H. Goerz, G. Gualdi, D. M. Reich, C. P. Koch, F. Motzoi, K. B. Whaley, J. Vala, M. M. Müller, S. Montangero, and T. Calarco, Optimizing for an arbitrary perfect entangler. II. Application, *Phys. Rev. A* **91**, 062307 (2015).
- [46] A. Gilchrist, K. Nemoto, W. J. Munro, T. C. Ralph, S. Glancy, S. L. Braunstein, and G. J. Milburn, Schrödinger cats and their power for quantum information processing, *J. Opt. B: Quantum Semiclass. Opt.* **6**, S828 (2004).
- [47] D. S. Schlegel, F. Minganti, and V. Savona, Quantum error correction using squeezed Schrödinger cat states, *Phys. Rev. A* **106**, 022431 (2022).